**SPECIAL TOPIC**

# Millennial-scale tree-ring isotope chronologies from coast redwoods provide insights on controls over California hydroclimate variability

Steven L. Voelker[1] · John S. Roden[2] · Todd E. Dawson[3]

## Abstract

To understand drivers of hydroclimate variability in north-coastal California, we obtained tree cross-sections from eleven coastal redwoods (mean age of 1232 years old) from the northern half of the species range. Tree rings from eight trees were cross-dated and sampled at sub-annual resolution for carbon isotope discrimination ($\Delta^{13}C$) and oxygen isotope composition ($\delta^{18}O$). Tree-ring $\Delta^{13}C$ and $\delta^{18}O$, compared to modern climate data, demonstrate these signals primarily record summertime hydroclimate variability—primarily through variables associated with evaporative conditions and/or precipitation. Our 1100-year stable isotope chronologies showed that north-coastal California did not undergo the megadroughts observed elsewhere in California and the western United States. This result implicates extended periods of low winter precipitation, rather than growing season evaporation, as the primary driver of previous megadroughts across California and neighboring regions. Compared to cool conditions prevailing over the Northern Hemisphere during the Little Ice age (1301–1875 of the common era, CE), the frequency of isotopic events of a certain magnitude was greater during periods with warmer Northern Hemisphere temperatures such as the Medieval Climate Anomaly (900–1300 CE) and the modern period (1876 to present). This association between tree-ring isotopic variability and long-term shifts in temperatures is consistent with the expected patterns in mid-latitude hydroclimate variability expected from arctic amplification (i.e., shifts in equator-to-pole temperature differences that modify jet stream speed and amplitude) or amplified quasi-resonant wave activity (i.e., wave-patterns in high-altitude winds that become "trapped" within a certain pattern, thereby producing a longer-duration periods of drought or wetness) across mid-latitudes during the boreal summer.

**Keywords** $\Delta^{13}C$ · $\delta^{18}O$ · Arctic amplification · Megadrought · Climate event frequency · Medieval climate anomaly · Little ice age

✉ Steven L. Voelker
dr.s.voelker@gmail.com

1 Department of Plants, Soils and Climate, Utah State University, Logan, UT, USA

2 Department of Biology, Southern Oregon University, Ashland, OR, USA

3 Department of Integrative Biology, University of California-Berkeley, Berkeley, CA, USA

## Introduction

For nearly 50 years carbon, hydrogen, nitrogen and oxygen stable isotopes in plants and plant materials have increasingly provided novel insights on plant ecophysiological responses to environmental variation. During this period, the Ehleringer research group has produced an astounding number of influential papers in this field (see a full list of nearly 500 papers, at the time of this writing, from the Ehleringer-group at http://ecophys.utah.edu/publications.html). Among a diverse menu of research projects, the Ehleringer group has contributed to advancing the theory and practice of how tree-ring isotopes can shed light on past environmental variation (Brooks et al. 1998; Roden and Ehleringer 1999; Roden et al. 2000; Barbour et al. 2004; Ward et al. 2002, 2005; Dawson et al. 2004; Roden and Ehleringer 2007). Here, we build upon these

foundational works to investigate whether low-frequency temperature variation over the past 1100 years has been associated with shifting isotopic variability in Coastal redwoods (*Sequoia sempervirens*).

In contrast to most dendrochronological collections that focus on tree species at higher elevations or inland locations, California redwoods occur within a narrow, ~50 km band adjacent to the California coastline where there is no snowpack to subsidize the prevailing rain-free summer conditions. Abundant wintertime precipitation recharges soil moisture each year in northern California's coastal forests, making this period extremely important to sustaining the hydrology and ecology of the region (Mooney and Dawson 2015). Due to this consistency of winter soil water recharge across northern California, the distribution of Coastal redwoods is thought to reflect summer atmospheric conditions and near-coastal ocean upwelling that strongly modify coastal cloud, fog and temperature regimes (Johnstone and Dawson 2010). Collectively, these climatic factors largely determine inter-annual variation in tree-ring carbon and oxygen isotope composition (Dawson 1998; Roden et al. 2009, 2011; Johnstone et al. 2013). Coastal redwoods can live to be more than 2000 years old and are readily accessible, but have long resisted efforts at dendrochronological dating (reviewed by Carroll et al. 2014). Carroll et al. (2014) succeeded in these efforts through extensive tree-climbing and increment core collection from upper canopy positions, where there are fewer rings that are "missing" or locally absent in some radii of the tree. Besides the inherent difficulty in climbing redwood trees, increment cores may not be long enough to extend over 1000 years in fast-growing trees and/or contain enough material in each ring for the analyses of multiple stable isotopes in slow-growing trees. For this research, we used an alternative approach, aimed at constructing a millennial length, sub-annual resolution tree-ring isotope chronologies from cross-sectional slabs from large old redwoods that had previously fallen over and died naturally.

Like other tree species, the "set-point" carbon stable isotope discrimination ($\Delta^{13}$C) in redwoods is largely determined by the ambient-to-leaf intercellular $CO_2$ concentration gradient (i.e., $c_a - c_i$) which, following Fick's law, is equivalent to the ratio of photosynthetic assimilation to stomatal conductance (i.e., $A/g_s$; see Ehleringer 1993). These basic physiological relationships can be translated into hypothetical climate effects on redwood tree-ring isotopes. In coastal California, summer conditions that are cloudy, foggy and wet would tend to promote higher $\Delta^{13}$C in redwoods through lower $A$ as driven by decreased irradiance, and greater $g_s$ as driven by lower leaf temperatures and associated leaf-to-air vapor pressure deficit (VPD), whereas sunny, warm and dry summer conditions with little fog would promote lower $\Delta^{13}$C. Indeed, our previous tree-ring isotope evidence documented coherence in these patterns within and across redwood stands (Roden et al. 2009, 2011; Johnstone et al. 2013).

Variation in tree-ring cellulose $\delta^{18}$O is largely controlled by how evaporative enrichment of leaf water and the isotopic signal of water vapor influence oxygen fixed in leaves and a partial re-exchange with xylem water where sugars are synthesized into tree-ring cellulose (Roden and Ehleringer 1999; Roden et al. 2000; Barbour et al. 2004). The dominant climatic factors affecting cellulose $\delta^{18}$O are temperature and relative humidity or VPD (Kahmen et al. 2011). However, redwoods can take up an enriched $\delta^{18}$O signature of fog through canopy-drip (Dawson 1998) as well as directly through leaves (Burgess and Dawson 2004; Burns Limm et al. 2009). Moreover, stable isotope theory indicates that under relative humidity values approaching 100% leaf water will undergo a near complete exchange with atmospheric water vapor. These conditions are most likely to occur under foggy conditions, where water vapor $\delta^{18}$O is also presumably enriched by the fog. Therefore, even leaves that stay dry during fog events can be presumed to be "labeled" by the fog-influence on the local water vapor $\delta^{18}$O. In summary, warm and dry conditions will always promote leaf water enrichment and higher tree-ring $\delta^{18}$O, but it is also possible that trees in areas regularly inundated by fog may also produce higher tree-ring $\delta^{18}$O during very foggy years. Our previous research suggested that leaf water evaporative enrichment associated with variation in summer VPD was the dominant signal recorded by redwood tree-ring $\delta^{18}$O (Johnstone et al. 2013).

A growing body of evidence suggests that anthropogenic warming has contributed to an intensification of climate extremes, including a greater frequency, persistence or severity of extreme weather/climate events (Fischer and Knutti 2015; Lehmann et al. 2015). Among the events partially attributed to global warming is dramatic hydroclimate variability affecting California from 2012 to 2017 (Williams et al. 2014; Wang et al. 2014; Diffenbaugh et al. 2015; Wang et al. 2017). The atmospheric dynamics characterizing such extreme events often defy our ability to attribute unequivocally the impact of recent anthropogenic warming. For robust attribution, the likelihood of events of a certain magnitude needs to have changed in a manner consistent with how climate dynamics are understood and how global climate models represent climate variability (Trenberth et al. 2015). An increased frequency of extreme weather/climate events in the Northern Hemisphere has been increasingly linked to "arctic amplification" and/or quasi-resonant planetary wave activity (Francis and Vavrus 2012; Coumou et al. 2014; Screen and Simmonds 2014; Petoukhov et al. 2016; Mann et al., 2017). Arctic amplification is characterized by greater warming at higher latitudes relative to lower latitudes which reduces the strength of northern hemisphere westerlies, thereby slowing the jet stream, increasing its

amplitude, and increasing climatic extremes (Francis and Vavrus 2012). Quasi-resonant amplification is characterized by waves in the Northern Hemisphere jet stream being "trapped" in a certain sequence that produces a higher likelihood of static weather conditions for longer periods during the boreal summer (Petoukhov et al. 2016). Other tree-ring isotope evidence suggests that El Niño Southern Oscillation (ENSO) activity has increased (Liu et al. 2017) which can ostensibly contribute to winter precipitation extremes across much of California (Cayan et al. 1999; McCabe and Dettinger 1999). It would, therefore, be of tremendous interest to identify climate proxies that can differentiate the influences of altered jet stream patterns and planetary wave activity versus ENSO dynamics for determining California hydroclimate variability. Towards this end, herein we use a unique coastal redwood data set to test whether isotopic variability, representing past hydroclimate variation, has shifted between the warmer modern period (i.e., the 1876 to present) of the Common Era (CE), the cooler Little Ice Age (LIA, 1301–1875 CE) as well as the warmer Medieval Climate Anomaly (MCA, 900–1300 CE).

## Methods

### Slab collection

Full or partial cross-sections from 11 dead and down trees and/or increment cores from five additional sites were collected between Humboldt Redwoods State Park (40.4°N) and as far as A.A. Loeb State Park in Oregon (42.1°N) at the northern range edge (Table 1). All previously fallen trees, which had previously been cut to clear a road, were sampled by permission from the Redwood State Parks and/or Redwood National Park. Slabs were cut using a 14-foot length cross-cut saw or using large chainsaws, in conjunction with parks personnel. Two to four slabs per trip were loaded into a cargo truck and transferred to Southern Oregon University for processing. See Figure S1 for images of slabs.

### Slab preparation

Slabs generally broke into many pieces upon being cut from down trees. Although the outer 50–200 years of sapwood was often decayed in trees dead more than 10–15 years, we were often able to locate sapwood that was preserved by the wet and low-oxygen conditions existing on the underside of the tree that was buried due to the considerable impact of the tree falling. Redwood slabs were surfaced flat using a hand-held electric planer and then dried in a processing laboratory. After the outer ~ 1 cm of wood was dry (complete drying took months), each slab was surfaced with a belt sander (Makita Corporation, Model 9403) with 80 and 120-grit paper, followed by an orbital sander with 220 and 320-grit paper. Areas of interest with small-rings were polished by hand with 400 and 600-grit sandpaper.

**Table 1** Characteristics of slabs and cores contributing to tree-ring width and stable isotope records for Redwood National and State Parks (S.P.)

| Site | ID | Slab diameter (m) | Earliest tree-ring year | Death date | Years cross-dated | Years used for isotope analyses |
|---|---|---|---|---|---|---|
| Redwood National Park | S1 | 1.4 | 1164 | 2010* | 1165–1640 | 1164–1489 |
| Del Norte Redwoods S.P. | S2 | 2.3 | 503 | 2008 | 550–2008 | 1488–2008 |
| Humboldt Redwoods S.P. | S3 | 2.9 | 450 | 1996 | 550–1996 | 942–1996 |
| Humboldt Redwoods S.P. | S4 | 3.2 | 551 | 2001 | 550–2001 | 855–1911 |
| Prairie Cr. Redwoods S.P. | S5 | 2.5 | 517 | 2010* | 550–1132 | 900–1132 |
| Prairie Cr. Redwoods S.P. | S6 | 3.1 | 1177 | 1950* | 1177–1888 | 1180–1871 |
| Prairie Cr. Redwoods S.P. | S7 | 2.9 | 1182 | 2004 | 1182–2004 | 1850–2004 |
| Prairie Cr. Redwoods S.P. | S8 | 2.2 | 866 | 1990* | 866–1947 | 900–1210 |
| Del Norte Redwoods S.P. | DN1192 | 2.1 | 1154 | 1970* | 1154–1713 | – |
| Humboldt Redwoods S.P. | RF3 | 2.3 | 117 | 2008 | 550–2008 | – |
| Humboldt Redwoods S.P. | RF4 | 1.6 | 721 | 2007 | 721–1300 | – |
| A.A. Loeb S.P. | Cores | – | – | – | 1885–2011 | 1890–2011 |
| Arcata Community Forest | Cores | – | – | – | 1960–2004 | 1960–2004 |
| Jedediah Smith Redwoods S.P. | Cores | – | – | – | 1952–2003 | 1952–2003 |
| Prairie Creek Redwoods S.P. | Cores | – | – | – | 1950–2003 | 1950–2003 |
| Del Norte Redwoods S.P. | Cores | – | – | – | 1495–2011 | – |

*Estimates to the nearest decade due to the outer section of the tree having been rotten and/or unable to be cross-dated due to the prevalence of locally absent rings during recent decades

## Tree-ring cross-dating and measurement

After sanding, slabs were visually assessed to identify all individual rings that could be located. These areas often occurred in a 10°–30° radial section that grew fastest at the height the slab was collected. However, even in this narrow area of fast growth, rings often "pinched out" (see Carroll et al. 2014) and went missing in one radii and then re-appeared in another radii. After identifying sections of the slab with the fewest locally absent rings, we conducted visual cross-dating among radii (after Yamaguchi 1991) where possible. However, many sections of 100 or more rings were so complacent that the only way to absolutely determine cross-dating was by tracing rings around the perimeter of the tree to other radii that had been assigned the same nominal year. After intra-tree cross-dating, we visually compared marker rings against chronologies composed of increment cores collected from younger living trees and/or other slabs as more of them were cross-dated against each other. Thereafter, tree-rings were measured, making note of radial shifts in the measurement path. To measure ring widths on pieces of wood that were too large for a conventional approach, we custom-mounted a binocular microscope with a counterbalance and affixed it to sliding stage interfaced with a linear encoder (Velmex Inc. "TA system", Bloomfield, NY) and MeasureJ2X software (Voortech Consulting) (measuring system shown in Figure S1). Ring-width series were then cross-dated among radii within a tree and then among trees using COFECHA software (Holmes 1983; Grissino-Mayer 2001) and Tellervo (Brewer 2014).

## Wood processing

Our goal was to cut each ring from at least four slabs per calendar year into three sections following sub-annual delineations determined in earlier studies (Roden et al. 2009; Johnstone et al. 2013). More specifically, the first ~15% of each ring was unused and disposed of whereas the middlewood (MW, central ~60% of the ring) and the anatomically distinct latewood (LW, outer ~25% of the ring) were collected for analyses. Wood sections were then cut out of the sanded cross-sections using a band saw. For all rings in slab 2, we used a robotic micro-mill and associated software (New Wave Research, Fremont, CA) for milling MW and LW sub-annual delineations within each tree ring. However, grinding enough wood for 459 years of MW and LW from this slab took approximately 1 year of operating the micro-mill for 4–8 h per day. This method was so time-consuming that we used multiple Dremel brand (Robert Bosch Tool Company, Gerlingen, Germany) rotary tools to grind all other rings, except for those <0.1 mm, for which the MW and LW components generally needed to be excised with a scalpel and binocular microscope.
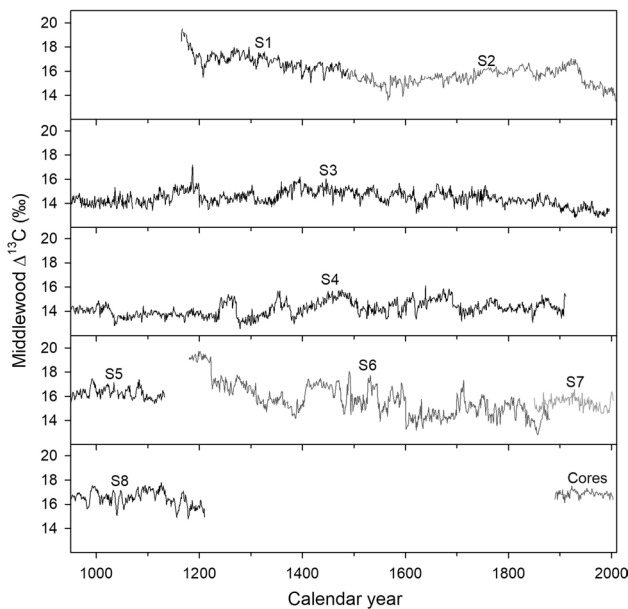
## Stable isotope analyses

Isotopic composition is expressed relative to that of a standard using "delta" notation as $\delta^{13}C = (R_{sample}/R_{standard} - 1) \times 1$ 000, where $\delta^{13}C$ is the molar ratio of heavy to light isotopes and $R_{standard}$ is Pee Dee Belemnite (PDB). The same notation holds for oxygen isotope composition except that $R_{standard}$ is VSMOW. Ground wood was heat-sealed within a polyester filter bag (mesh size 25 μm, ANKOM Technology, Macedon, NY) and extracted to α-cellulose (Leavitt and Danzer, 1993; Sternberg, 1989). Thereafter, two replicates of alpha-cellulose were weighed out on a microbalance (~0.20 mg per replicate) for each of MW$\delta^{13}$C, LW$\delta^{13}$C and LW$\delta^{18}$O (i.e., at least six replicate analyses per ring). Funding limitations required us to forego analyses of MW$\delta^{18}$O. The carbon isotope ratio of each sample was obtained using standard high temperature combustion in a vario-Pyrocube elemental analyzer interfaced with IsoPrime/Elementar IsoPrime 100 gas phase isotope ratio mass spectrometer (IsoPrime Ltd., Manchester, UK). The oxygen isotope ratios were determined by pyrolyzing α-cellulose in an elemental analyzer (TC/EA, IsoPrime/Elementar vario-Pyrocube) and analyzing the resulting gas with an isotope ratio mass spectrometer (IsoPrime100) at the Roden or Dawson laboratories at Southern Oregon University or UC-Berkeley, respectively. At both laboratories, the long-term precision does not exceed ±0.1‰ for $\delta^{13}$C and 0.2‰ for $\delta^{18}$O. The data from each tree/isotope combination were always run at a single lab and the same working standards were used in both laboratories to ensure that isotopic data were comparable among trees without further standardization.

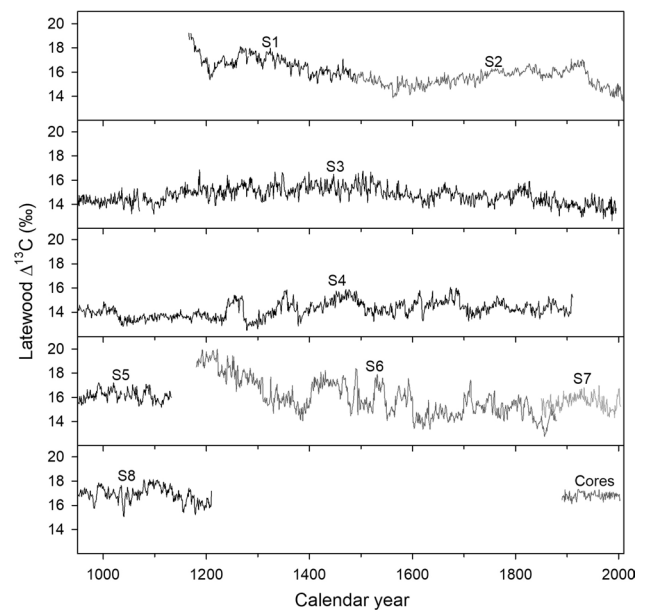## Processing of stable isotope time-series data

All $\delta^{13}$C values were converted to carbon isotope discrimination values ($\Delta^{13}$C) to remove shifts in $\delta^{13}C_{air}$ that have been driven by fossil-fuel burning. The calculation of $\Delta^{13}$C followed Farquhar et al. (1982): $\Delta^{13}C = (\delta^{13}C_{air} - \delta^{13}C_{plant})/(1 + \delta^{13}C_{plant}/1000)$, where $\delta^{13}C_{air}$ was estimated annually from the values given by McCarroll and Loader (2004) merged with more recent $\delta^{13}C_{air}$ records from Mauna Loa, Hawaii. In some cases, tree-ring stable isotope series may need no detrending. Indeed, relatively short time-series of $\Delta^{13}$C and $\delta^{18}$O data from younger redwood trees did not previously need to be detrended prior to produce reliable series inter-correlation values and strong correlations with climate data (Roden 2008; Johnstone et al. 2013). However, the redwoods sampled for those previous studies were younger trees that have larger rings and have yet to undergo large canopy gap-formation events or other disturbances such as intense wildfires and/or twentieth century road-building adjacent to the sample trees.

Due to the step changes in raw $\delta^{18}O$ values for slab S3 near 1746, 1766 and 1790, that could not be captured by even the most flexible detrending splines, we broke this time-series into four separate shorter time-series (Fig. 3, see "Results" and "Discussion" for interpretation). A single time-series was then composed of the constituent, indexed time-series. The resulting time-series was then converted back to per mil values with a mean and inter-annual standard deviation calculated matching each of the constituent time-series without step changes. As noted above, the tree-ring isotope time-series obtained from old-growth trees had been influenced by local, non-climate processes that caused decadal to centennial-scale shifts in isotopic values (Figs. 1, 2, 3). Therefore, using the program ARSTAN (Cook and Krusic 2014) we determined that for $\Delta^{13}C$, a flexible spline of < 30 years maximized series inter-correlation whereas for $\delta^{18}O$, more rigid splines of up to 100 years or more preserved the same series inter-correlation values as more flexible splines. As a result, both $\Delta^{13}C$ data and $\delta^{18}O$ data were detrended with a 50-year spline that emphasized inter-annual variability but also retained decadal-scale variability.

For further analyses, we obtained the individual detrended time-series for each slab after ARSTAN detrending. We chose to use "ARSTAN time-series" rather than pre-whitened time-series (i.e., all autocorrelation removed from a series) because some aspects of modern and presumably pre-instrumental hydroclimate variability in this region include low-frequency signals and associated persistence that we wanted to retain in our isotopic records.
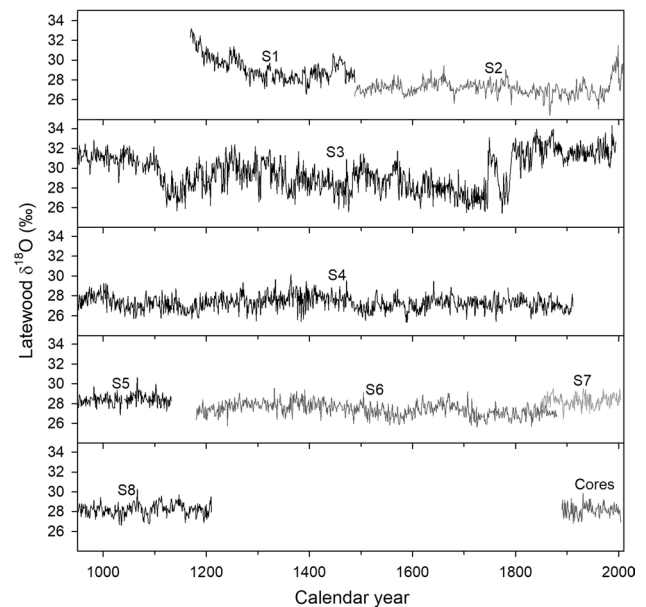


**Fig. 2** Time-series of carbon isotope discrimination values of latewood cellulose from eight redwood slabs and composited core collections. Data shown were not indexed or detrended, but data for cores were averaged into a single chronology

To produce a chronology with the strongest climatic signal, we closely inspected individual detrended series that had inter-correlation values < 0.1 and removed those that were clearly different than the remaining constituent series due to local non-climate effects or a potential mistake in sample



**Fig. 1** Time-series of carbon isotope discrimination values of middlewood cellulose from eight redwood slabs and composited core collections. Data shown were not indexed or detrended, but data for cores were averaged into a single chronology



**Fig. 3** Oxygen isotope values of latewood from eight redwood slabs and core collections. Data shown were not indexed or detrended, but data for cores were averaged into a single chronology

processing that altered the initial cross-dating based on ring-width data. To construct the final stable isotope chronologies used in the analyses reported here, we calculated arithmetic means for each year from the remaining isotope time-series (Figure S2).

## Statistical analyses

The analyses employed to revisit how stable isotope signals record hydroclimate variability, after Johnstone et al. (2013) were first assessed using Pearson correlation analyses (Table S1). Thereafter, we conducted multiple regression analyses by employing 'lm' and 'step' functions in R (R Core Team 2017) (Table S2). We deemed it infeasible to produce a conventional climate reconstruction that yields a certain meteorological value for any given year since many different aspects of hydroclimate affect coastal redwood isotope signals and much of the millennial time-series contained a sample depth of four or fewer trees. To avoid such uncertainty for any given year, we assessed isotopic variability across many years by calculating the frequency in which isotopic variability met a certain threshold standard deviation, or $Z$ score. This follows the guidance of Trenberth et al. (2015) on how to identify shifts in climatic variability associated with climate change. Extreme climate events (i.e., events with an SD > 2), by definition, do not occur very frequently, which can make it impossible to accurately assess the likelihood of extreme event occurrence, even across a long time-series. Moreover, because stable isotopes record climatic conditions at time-scales of approximately 3–5 months (Tables S1 and S2), it is likely that extreme weather events lasting < 4 months would be somewhat attenuated in the isotopic record. We, therefore, assessed the frequency of isotopic variability of ± 0.8, ± 1.0 or ± 1.2 SD events using two-proportion $Z$ tests across long time periods previously identified as being associated with shifts in Northern Hemisphere temperatures. These included the modern period (MOD, 1876–2004 CE) the Little Ice Age (LIA, 1301–1875 CE) and the Medieval Climate Anomaly (MCA, 900–1300 CE). To visualize how multidecadal to centennial-scale patterns in event frequency compared to Northern Hemisphere temperatures, we calculated moving averages. The moving average of event frequency (200 years) is necessarily longer than that for the paleotemperature record (50 years) because isotopic event frequency, by definition, has fewer observations across a given time period and is necessarily more variable due to values nearest to the mean having been removed. To supplement these analyses of isotopic event frequency, and to better identify when certain frequency domains may be present across the past 1100 years, we also provide visualizations of a continuous wavelet transform analyses (Figure S4A–E), conducted

for each stable isotope chronology using the dlR package (Bunn 2008; Bunn et al. 2018).

## Results

As we processed and analyzed tree-ring stable isotope data from each redwood slab over the course of the project, it became progressively clearer that factors besides climate had strongly influenced some redwood trees whereas others displayed little such multi-decadal to centennial-scale variation. For example, developmental declines in carbon isotope discrimination that likely owe to increasing tree height and/or a progressively more dominant canopy position in Slab S1 and Slab S6 (Figs. 1, 2). In some slabs like S3, there was little evidence for multi-decadal shifts in $\Delta^{13}$C, whereas there was considerably greater multi-decadal variation in S4, which was located just a few hundred meters distance from S3 in the Bull Run watershed of Humboldt Redwoods State Park, (Figs. 1, 2). The greatest multi-decadal shifts in $\Delta^{13}$C were found in Slab 6, which was located near the Prairie Creek Redwoods State Park visitor center. Interestingly, although-multi-decadal variation in LW$\delta^{18}$O did occur, it rarely reflected the multi-decadal shifts in LW$\Delta^{13}$C for the same tree. For example, slab S1 appears to include a developmental trend in LW$\delta^{18}$O that is consistent with a similar decline in LW$\Delta^{13}$C, whereas the LW$\delta^{18}$O record of Slab S6 shows no developmental shift and very little in the way of multi-decadal shifts observed in its LW$\Delta^{13}$C record (Figs. 2, 3). The most striking shifts in LW$\delta^{18}$O are those preserved in Slab S3 (Fig. 3). From 1745 to 1749, there was a peak enrichment of 7.2‰, which subsequently diminished over the next few decades, with the greatest decrease being a 5.6‰ depletion from 1763 to 1774. Soon after, there was another abrupt period of enrichment of up to 6.3‰ from 1784 to 1796, with the greatest portion of that pulse occurring from 1789 to 1795. Yet, again, there were no corresponding shifts in LW$\Delta^{13}$C for this same period of multi-decadal volatility in LW$\delta^{18}$O, suggesting neither shifts in the canopy environment and/or leaf gas-exchange could have explained these observations. We conducted four or five replicate analyses for each tree-ring year across these shifts to confirm that variation in LW$\delta^{18}$O was not due to analytical error.

Our previous work indicated that having both LW$\Delta^{13}$C and LW$\delta^{18}$O signals agree on the sign-reversed magnitude of an event-year more accurately defined the hydroclimatic regime of a given summer as being generally wet or dry (Johnstone et al. 2013). More specifically, low $\Delta^{13}$C and high $\delta^{18}$O equated to dry conditions, fewer clouds and high vapor pressure deficit (VPD), whereas high $\Delta^{13}$C and low $\delta^{18}$O equated to wetter conditions, more clouds and lower VPD. We revisited these analyses after incorporating our

new, overlapping stable isotope data and found MW$\Delta^{13}$C and LW$\Delta^{13}$C and LW $\delta^{18}$O were all consistently affected by regional evaporative conditions, precipitation or a combination of these variables during summer (Table S1, S2). Although correlations between the isotope chronologies and any individual climate variable were not particularly strong ($R^2 \leq 0.3$, Table S1), multiple regression using three to six summer hydroclimate variables predicted far more of the variation in stable isotope chronologies ($R^2 = 0.27$–0.58, Table S2). Therefore, our stable isotope chronologies robustly represent summer hydroclimate variability across north-coastal California. Because LW$\Delta^{13}$C and LW $\delta^{18}$O stable isotope chronologies represent overlapping climate influences (Table S1, S2), we plotted these together for comparison (Fig. 4b) and then combined these into a single $Z$ score index that equally weights variation in each isotope for each year (Fig. 4c). Some individual years and small groups of approximately two to five years have very low (or high) $Z$ score index values, ostensibly indicative of dry (or wet) events (Fig. 4c). However, perhaps the most striking aspect of these data is the *lack* of decadal to multi-decadal "mega-droughts" in this record compared to most other regions in

the western United States (Stahle et al. 2000; Cook et al. 2010; Meko et al. 2012; DeRose et al. 2015).

Rather than quantify the magnitude of a particular climate variable in any given year, our goal was to detect shifts in isotopic variability, with the knowledge that such shifts would be representative of a collection of climate variables impacting hydroclimate variability. However, we were uncertain to what extent synoptic scale climate variability (approximately 1–10 days, Vinnichenko 1970), may be recorded by climate proxies that record climate conditions averaged over 1 month or more. Therefore, we conducted a numerical exercise as a proof of concept (Figure S3). This exercise consisted of 100 sets of randomly generated daily air temperature data that were each 100 years in length and set to a mean of 23°C. Across these 100 years, the day-to-day variance of air temperature was set to double. Daily temperature data were averaged across 50 or 100 days to represent the time scales at which our climate proxies may preserve climatic information. On average, inter-annual variation in these 50- or 100-day means retained about two-thirds of the shift in variance imposed at the daily scale. Therefore, although a sub-seasonal climate proxy cannot diagnose the strength of a particular synoptic scale weather event, this exercise demonstrated that shifts in synoptic scale variability should still be retained in our stable isotope records.

Indeed, centennial-scale shifts in the frequency of wet and dry MW$\Delta^{13}$C events demonstrated that early growing season weather/climate was significantly more variable during the Medieval Climate Anomaly (MCA) and the modern period compared to the Little Ice Age (LIA) and these patterns correspond to low-frequency variation in average temperatures across the Northern Hemisphere (Table 2; Fig. 5a). The same assessment of wet and dry event frequency, except this time in years where both LW$\Delta^{13}$C and LW$\delta^{18}$O recorded the same event magnitude, provides additional evidence that late growing season weather/climate variability was also more variable during the MCA and the modern period compared to the LIA (Table 2; Fig. 5a). Although the difference in event magnitude frequency between the MCA and LIA was greater for the late growing season compared to the modern period vs the LIA (Table 2) the low-frequency trends in event frequency more closely tracked Northern Hemisphere temperatures (Fig. 5b). Wavelet analyses indicated that there were significant components of variation in MW$\Delta^{13}$C and LW$\Delta^{13}$C that ranged from 10 to 40 years on average, a range of decadal to multi-decadal variability ostensibly similar to the PDO-like signal, and that this low-frequency variation was weakest or absent during the peak of the LIA, from 1650 to 1900 (Figures S4A–C). LW$\delta^{18}$O did not show this low-frequency variation as consistently throughout the record, but did contain some evidence for greater low-frequency variation during the MCA and recent
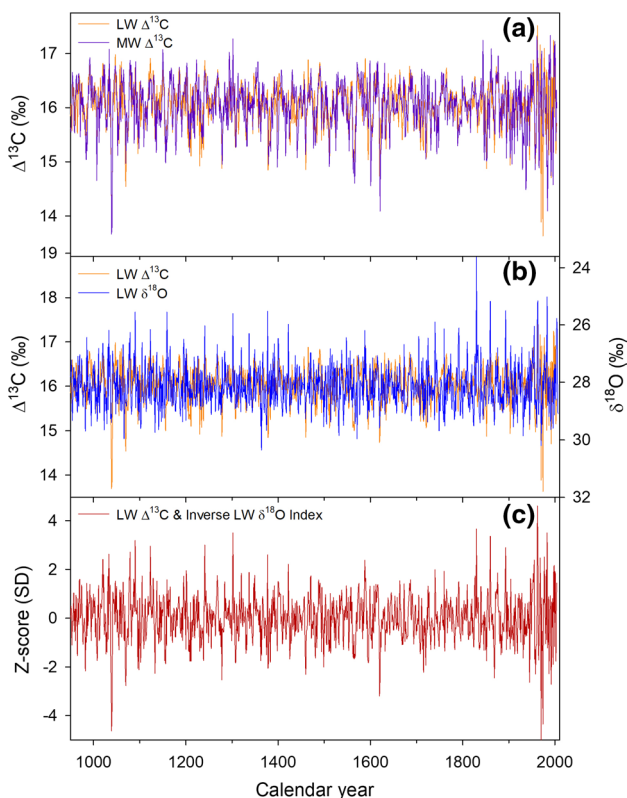


**Fig. 4** Detrended chronologies of middlewood (MW) and latewood (LW) carbon isotope discrimination values ($\Delta$) and LW oxygen isotopes ($\delta^{18}$O, note that axis values are reversed) and an index chronology that averaged LW$\Delta$ and inverse LW$\delta^{18}$O $Z$ scores (color figure online)

**Table 2** Probability values associated with a two-proportion $Z$ test comparing the frequency of events meeting a threshold isotopic $Z$ score (i.e., frequency of wet and/or dry events) among three time periods; the modern period (MOD, years = 1876–2004) the Little Ice Age (LIA, years = 1301–1875) and the Medieval Climate Anomaly (MCA, years = 900–1300)

| Time period comparison | Threshold isotopic $Z$ score | MW$\Delta$ | LW$\Delta$ | LW$\delta^{18}$O | LW$\Delta$ and LW$\delta^{18}$O |
|---|---|---|---|---|---|
| MCA vs LIA | 1.2 SD | **0.005** | 0.173 | 0.171 | **0.007** |
| LIA vs Mod | | **0.008** | 0.058 | 0.305 | 0.142 |
| Mod vs MCA | | 0.288 | 0.197 | 0.555 | 0.726 |
| MCA vs LIA | 1 SD | **0.008** | 0.206 | 0.303 | **0.012** |
| LIA vs Mod | | **0.023** | 0.157 | 0.118 | 0.206 |
| Mod vs MCA | | 0.372 | 0.341 | 0.217 | 0.751 |
| MCA vs LIA | 0.8 SD | **0.022** | 0.165 | 0.394 | **0.034** |
| LIA vs Mod | | **0.026** | 0.135 | 0.243 | **0.040** |
| Mod vs MCA | | 0.310 | 0.342 | 0.312 | 0.345 |

Probability values of < 0.05 are in boldface type
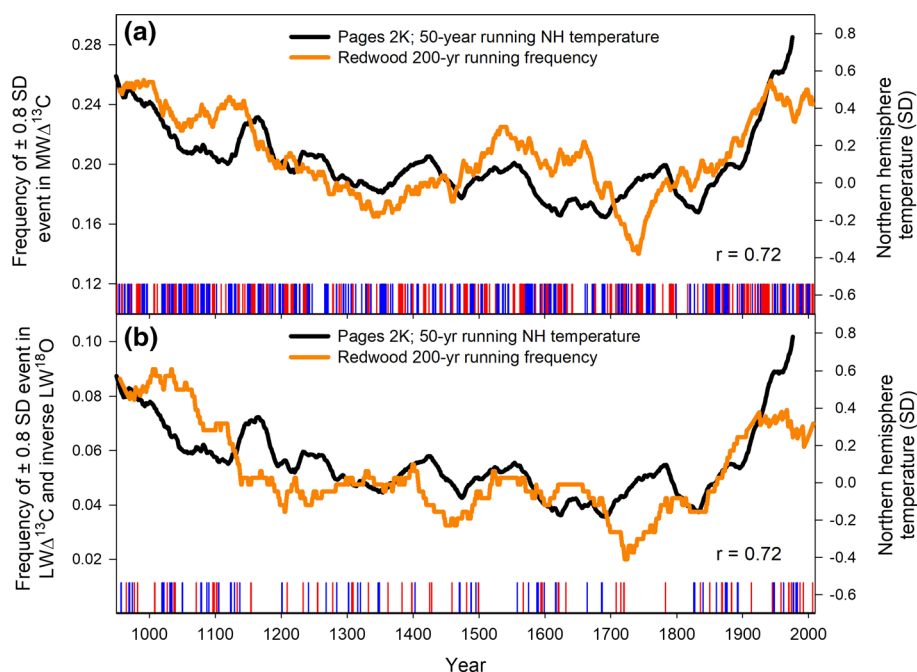


**Fig. 5** The frequency of events meeting a threshold isotopic $Z$ score of ± 0.8 SD for middlewood carbon isotope discrimination (MW$\Delta$) and the frequency of both latewood (LW) $\Delta$ and LW$\delta^{18}$O both having a ± 0.8 SD $Z$ scores in opposite directions for the same year. Opposing isotopic signals convey an agreement on either of wet or dry conditions (blue or red bars on the bottom of each panel). A running 200-year average of this frequency is shown as an orange line. The frequency of events shows broad agreement with a 50-year running average of the mean Northern Hemisphere temperatures in units of standard deviations (PAGES 2k Network; mean of Arctic, Asia, Europe and North American records). This indicates that growing season coastal climate conditions were more variable during the warm Medieval Climate Anomaly (900–1300 CE) and the modern period (1876–2004 CE) compared to lower variability during the Little Ice Age (1301–1875 CE). Note that the running frequency is calculated over progressively smaller intervals after 1905, culminating in the frequency value for 2004 only sampling over the period 1905–2004 (color figure online)

decades (Fig S4D). The combined LW$\Delta^{13}$C, LW$\delta^{18}$O chronology showed the strongest evidence of more multi-decadal variation being almost exclusively present during the MCA and the modern period (Figure S4E). In summary, despite the challenge of necessarily few trees having been sampled for isotopic variation in any given year, the millennial length inter-annual records of MW$\Delta^{13}$C, LW$\Delta^{13}$C and LW$\delta^{18}$O allowed us to determine that (1) multi-decadal megadroughts are exceedingly rare or simply absent in north-coastal California, (2) the frequency of isotopic events of a certain magnitude was greater during the MCA and modern period and lower during the LIA, and (3) these shifts in isotopic event frequency may have interacted with the presence or absence of low-frequency variation in hydroclimate.

## Discussion

Tree-ring stable isotopes provide a unique record of a tree's ecophysiological responses to environmental and climate variability (McCarroll and Loader 2004). The climatic setting that coastal redwoods reside (Johnstone and Dawson 2010) results in inter-annual variation in $MW\Delta^{13}C$ and $LW\Delta^{13}C$ having been determined by how summer fog, clouds and VPD affect both photosynthetic assimilation to stomatal conductance in the same direction (Johnstone et al. 2013; Tables S1, S2). These climate signals are similar to other millennial-length isotope records from coastal or near-coastal locations (Young et al. 2012; Loader et al. 2013). Although coastal fog provides an enriched water isotopic signature to redwoods locally (Dawson 1998), large-scale synoptic conditions that influence summer VPD, precipitation and other variables related to summer hydroclimate variability largely determine inter-annual variation in tree-ring $\Delta^{13}C$ and $\delta^{18}O$ (Johnstone et al. 2013; Tables S1, S2). Indeed, these patterns are what would be expected from detailed physiological studies underlying mechanistic models of $\Delta^{13}C$ and $\delta^{18}O$ from plant material (Farquhar et al. 1982; Ehleringer 1993) and $\delta^{18}O$ (Roden and Ehleringer 1999; Roden et al. 2000; Barbour et al. 2004; Kahmen et al. 2011). In turn, application of this knowledge and sub-annual stable isotope analyses to the first millennial-length cross-dating of coastal redwood tree-rings (Carroll et al. 2014 and this study) has provided powerful new insights on the past hydroclimate variation across California.

### Insights on isotopic and California hydroclimate variability

The strength and position of the high-pressure ridge located off the Pacific coast of North America is a dominant atmospheric feature that has influenced winter precipitation patterns and intensity during the modern period across the western United States (Wang et al. 2014; Seager et al. 2015; Wang et al. 2017). These same features presumably operated during the eleventh- and sixteenth century, when dendrochronological records indicate that megadroughts occurred across central to northern California (Stahle et al. 2000; Cook et al. 2010; Meko et al. 2012; Malevich et al. 2013). However, Malevich et al. (2013) noted that the severity of the sixteenth century drought was substantially less across northern compared to central California. Our data further clarify that both of these ancient megadroughts had little impact on north-coastal California. The lack of megadroughts for the north-coast has been recently underscored by how this region

underwent a moderate drought during 2012–2015 while the rest of the state experienced drought conditions that were severe to unprecedented in the past 1000+ years (Griffin and Anchukaitis 2014; Williams et al. 2014; Robeson 2015). The recent severe drought has resulted in massive tree mortality across much of the California (Asner et al. 2016; Young et al. 2017). For example, from 2012 to 2015 the June–September Palmer Drought Severity Index (PDSI) for the North-Coastal climate division was only $-1.93$ whereas all other California climate divisions had PDSI values that were at least $-2.9$, and as low as $-4.4$ to $-4.5$ for the Central Coast and San Joaquin climate divisions. The projected effects of modern climate change on terrestrial ecosystem water availability have prompted increasing concern for identifying hydrological refugia or micro-refugia for plants, particularly for trailing-edge populations (McLaughlin et al. 2017). The lack of evidence for megadroughts and the attenuated effects of the 2012–2015 California Drought suggest that the north coast of California may provide a relatively stable macro-refugia. As such, conservation concerns for coast redwoods and other coastal forests in this region will likely become all the more important as climate change reduces the viable niche space for many species elsewhere in California.

The lack of isotopic evidence for long-past megadroughts does not necessarily indicate cool-season precipitation deficits did not also occur along the north-coast, since even relatively dry winters are still characterized by a threshold level of precipitation that redwood ecophysiology and associated isotopic signals cannot differentiate from winters with abundant precipitation. Rather, the lack of a megadrought signal in coast redwoods is best explained by these trees recording summer conditions almost exclusively (Johnstone et al. 2013; Tables S1, S2) whereas climate proxies based on tree-ring widths from this region are dominated by winter precipitation signals (Malevich et al. 2013; Griffin and Anchukaitis 2014; Belmecheri et al. 2016). Differences in climate proxy seasonality can mostly be attributed to the more dependable winter rainfall in north-coastal California and to a lesser extent on how high summer temperatures affecting interior California, Oregon and Washington can promote greater inland-advection of cool marine-layer air and fog (Johnstone and Dawson 2010). These climatological patterns and our stable isotope chronologies collectively imply that the eleventh and sixteenth century megadroughts were caused primarily by a series of years with low winter precipitation, the seasonality of which could not have been identified previously with tree-ring records alone. In contrast, anomalously low winter precipitation and warmer year-round temperatures contributed to the unprecedented severity of the 2012–2015 California drought (Williams et al. 2014; Diffenbaugh et al. 2015; Seager et al. 2015).

Following the conceptual framework of Trenberth et al. (2015), we found that the isotopic variability (i.e., the likelihood of events of a certain magnitude) was greater during the MCA and modern period compared to LIA (Table 2). Indeed, the multi-centennial to millennial-scale agreement between these isotopic event frequencies and temperature-sensitive tree-ring growth patterns (Fig. 5) underscores the importance of past shifts in Northern Hemisphere and tropical volcanic activity and associated solar irradiance as well as changes in greenhouse gas-forcing (Vieira and Solanki 2010; Pages 2k Network 2013; Sigl et al. 2015). Moreover, there are likely connections between these patterns in likelihood of isotopic event frequency and parallel shifts in lower-frequency variability in summer hydroclimate (Figures S4A–E). Further data and analyses are required to better isolate how decadal to multi-decadal variation in hydroclimate (Figures S4A-E) may have contributed to the broad shifts in the likelihood of isotopic event frequency that parallel changes in Northern Hemisphere temperatures between the MCA, LIA and the modern period (Table 2; Fig. 5). It is consequential that trends in the running frequency of $MW\Delta^{13}C$ events and the agreement between $LW\Delta^{13}C$ and $LW\delta^{18}O$ events closely track one another. Redwood $MW\Delta^{13}C$ chronologies are more influenced by variation in early summer temperatures and evaporative conditions, whereas $LW\Delta^{13}C$ and $LW\delta^{18}O$ are influenced by a combination of summer evaporative conditions and precipitation (Table S1, S2). Therefore, we conclude broad-scale atmospheric conditions that collectively modify summer VPD, cloudiness and precipitation is the primary control on redwood tree-ring isotopic variability.

ENSO phase often affects winter precipitation across California (McCabe and Dettinger 1999; Cayan et al. 1999). Therefore, millennial-length records of ENSO variability (Liu et al. 2017) and the position of the Intertropical Convergence Zone (Higley et al. 2018) would not be expected to directly affect summer hydroclimate conditions recorded by isotopes in coast redwoods. Although the PDO influences summer ocean temperatures and fog occurrence, PDO phase is primarily controlled by a complex interaction of tropical sea surface temperatures and mid-latitude atmospheric circulation, which makes it difficult to assess the potential for past PDO variation to have modified centennial- to millennial-scale hydroclimate variability for north-coastal California (McAfee 2016; Newman et al. 2016). Given the lack of teleconnections that could influence summer hydroclimate in California, arctic amplification (Francis and Vavrus 2012) and/or the resonance of planetary waves (Petoukhov et al. 2016) can be considered as the most likely drivers of low-frequency shifts in isotopic variability a that are broadly similar to patterns in Northern Hemisphere temperatures (Fig. 5; Table 2). Arctic amplification occurs in boreal summer because this period is when poleward temperature gradients and associated jet stream velocities are lowest. Wave resonance is caused by westward-propagating planetary waves being "trapped" in a certain configuration or latitudinal waveguide, which may be linked to arctic amplification (Kornhuber et al. 2016; Petoukhov et al. 2016; Mann et al. 2017). Either or both phenomena provide viable mechanistic explanations for how extreme or long-duration summer temperature or precipitation events may become more common under warmer climates (Screen and Simmonds 2014; Coumou et al. 2015; Fischer and Knutti 2015; Lehmann et al. 2015). Mann et al. (2017) indicated that "models and observations suggest that this signal has only recently emerged from the background noise of natural variability". Our data provide compelling evidence for these phenomena having been operational and linked to low-frequency Northern Hemisphere temperature variability over the past 1100 years.

The strongest divergence between redwood isotopic event frequency and Northern Hemisphere temperatures apparently occurs during recent decades (Fig. 5). However, this pattern is likely an artifact of tree-ring isotope records extending through 2004, which requires an increasingly shorter running window of isotopic event frequency. In other words, the value plotted for 2004 only represents isotopic variability from 1905 to 2004 and omits 100 years of variability after this date. The trend in isotopic event frequency would more closely follow recent temperature trends if it had included upticks in hydroclimate variability since 2004 (Screen and Simmonds 2014; Fischer and Knutti 2015; Lehmann et al. 2015; Horton et al. 2016) as well as climate-model projections of further amplified hydroclimate variability (Yoon et al. 2015).

## Lessons about the past lives of old-growth redwoods

Old redwoods have persisted through periods that were far more dynamic than we might realize when casually strolling beneath these trees on park roads and groomed trails. Indeed, redwood tree-ring isotope series showed decadal-to multi-decadal shifts that were rarely shared among slabs and, therefore, must have been driven by responses to disturbance. The most common disturbances affecting tree-ring isotopes would include a changing canopy light-environment, due to an adjacent tree having fallen over or when fires locally burned into the canopy—which is widely evident in redwood forests by the prevalence of charred bark far up into the canopy of redwood trees. The most peculiar isotopic variation observed was that of $LW\delta^{18}O$ of slab 3 during the 1700 s, which included dramatic pulses in isotopic variability. This tree was located on an alluvial flat, only 20–30 m distance from the current active channel of Bull Run Creek. Therefore, we suspect that variation owes

to a flood having deposited a thick layer of sediment around the base of the tree that altered the local soil hydrology; thereafter, this sediment was scoured away over ~25 years only for another flood to redeposit more sediment and again modify the local soil hydrology. This flooding hypothesis is supported by evidence from a reconstruction of the Sacramento River (Meko et al. 2001). Meko et al. (2001) identified the 1745 water year as the 6th greatest discharge year in the past ~1100 years, and this happens to correspond to the initial year of the first upward pulse in LW$\delta^{18}$O of slab 3. Likewise, the second upward pulse in LW$\delta^{18}$O peaked after 1789, which corresponds to Sacramento River discharge reconstructions ranked 21st and 16th in 1789 and 1790, respectively. Indeed, these pulses in LW$\delta^{18}$O are so large that it may be possible to use decadally resolved LW$\delta^{18}$O from redwoods growing adjacent to rivers to identify the approximate timing of shifts and thereafter to sample annually over selected years to identify the exact years of past massive flood events. Slab 2 was from a very old and large tree (~3 m in diameter at the base) in Del Norte Redwoods State Park that was apparently left standing by loggers even though the surrounding forest was clear-cut sometime in the early 1970s. Slab 2 shows a ~2 ‰ increase in LW$\delta^{18}$O corresponding to the time of clear-cutting, but little change to $\Delta^{13}$C (Figs. 2, 3). Slab 2 and Slab 3 thus demonstrate the near necessity of detrending long isotope series to remove the effects of stand dynamics or shifts in hydrology in old-growth coastal redwoods.

## Conclusion

Determining what climate signals are contained in tree-ring isotopes of coastal redwoods has been a process, our group has advanced over the past 20 years (Dawson 1998; Roden et al. 2009; Johnstone et al. 2013; Table S1). This progress rests upon important insights from the Ehleringer research group that demonstrated a wide range of mechanistic controls on isotopic signals in plants (Dawson and Ehleringer 1991; Flanagan et al. 1991; Comstock and Ehleringer 1992; Ehleringer 1993; Ehleringer and Cerling 1995; Sparks and Ehleringer 1997; Roden and Ehleringer 1999; Roden et al. 2000; Barbour et al. 2004; Tipple et al. 2013). Here, we have extended this tradition to gain insights on the past hydroclimate of California. Our evidence suggests strongly that north-coastal California has been free from the multi-decadal megadroughts that have affected the large areas of the western United States—thereby identifying winter precipitation anomalies as the primary factor in previous megadroughts. The lack of megadroughts in this region also suggest that it has and will continue to function as a stable hydrologic refugia (sensu McLaughlin et al. 2017). Shifts in inter-annual variability of the tree-ring isotope records are

consistent with hydroclimate variability of this region having tracked low-frequency trends in Northern Hemisphere temperatures. Due to the lack of known teleconnections that could strongly influence boreal summer hydroclimate variability for this region, we conclude that the long-term shifts in isotopic event frequency across the past 1100 years provide evidence for past Northern Hemisphere temperature trends being linked to patterns in atmospheric circulation through arctic amplification and/or quasi-resonant planetary wave dynamics.

**Author contribution statement** JSR and TED conceived of the research, oversaw and contributed to the research. SLV oversaw data collection, analyzed the data and wrote the manuscript. JSR and TED provided editorial advice.

## References

Asner GP, Brodrick PG, Anderson CB, Vaughn N, Knapp DE, Martin RE (2016) Progressive forest canopy water loss during the 2012–15 California drought. Proc Natl Acad Sci USA 113:E249–E255

Barbour MM, Roden JS, Farquhar GD, Ehleringer JR (2004) Expressing leaf water and cellulose oxygen isotope ratios as enrichment above source water reveals evidence of a Péclet effect. Oecologia 138:426–435

Belmecheri S, Babst F, Wahl ER, Stahle DW, Trouet V (2016) Multi-century evaluation of Sierra Nevada snowpack. Nat Clim Change 6:2–3

Brewer PW (2014) Data management in dendroarcheology using Tellervo. Radiocarbon 56:S79–S83

Brooks JR, Flanagan LB, Ehleringer JR (1998) Responses of boreal conifers to climate fluctuations: indications from tree-ring widths and carbon isotope analyses. Can J For Res 28:524–533

Bunn AG (2008) A dendrochronology program library in R (dplR). Dendrochronologia 26:115–124

Bunn AG, Korpela M, Biondi F, Campelo F, Mérian P, Qeadan F, Zang C, Buras A, Cecile J, Mudelsee M, Schulz M, Pucha-Cofrep D, Wernicke J (2018) dplR: dendrochronology Program Library in R. R package version 1.6.7. http://R-Forge.R-project.org/projects/dplr/

Burgess SSO, Dawson TE (2004) The contribution of fog to the water relations fo Sequoia sempervirens (D. Don): foliar water uptake and prevention of dehydration. Plant Cell Environ 27:1023–1034

Burns Limm E, Simonin KA, Bothman AG, Dawson TE (2009) Foliar water uptake: a common water acquisition strategy for plants of the redwood forest. Oecologia 161:449–459

Carroll AL, Sillett SC, Kramer RD (2014) Millennium-scale crossdating and inter-annual climate sensitivities of standing California redwoods. PLoS ONE 9:e102545

Cayan DR, Redmond KT, Riddle LG (1999) ENSO and hydrologic extremes in the western United States. J Clim 12:2881–2893

Comstock JP, Ehleringer JR (1992) Correlating genetic variation in carbon isotopic composition with complex climatic gradients. Proc Natl Acad Sci 89:7747–7751

Cook ER, Krusic PJ (2014) ARSTAN version 44h3: A tree-ring standardization program based on detrending and autoregressive time series modeling, with interactive graphics. Tree-Ring Laboratory, Lamont-Doherty Earth Observatory of Columbia University, Palisades

Cook ER, Seager R, Geim RR Jr, Vose RS, Herwiejer C, Woodhouse C (2010) Megadroughts in North America: placing IPCC projections of hydroclimatic change in a long-term paleoclimate context. J Quat Sci 25:48–61

Coumou D, Petoukhov V, Rahmstorf S, Petri S, Schellnhuber HJ (2014) Quasi-resonant circulation regimes and hemispheric synchronization of extreme weather in boreal summer. Proc Natl Acad Sci 111:12331–12336

Coumou D, Lehmann J, Beckmann J (2015) The weakening summer circulation in the Northern Hemisphere mid-latitudes. Science 348:324–327

Dawson TE (1998) Fog in the California redwood forest: ecosystem inputs and use by plants. Oecologia 117:476–485

Dawson TE, Ehleringer JR (1991) Streamside trees that do not use stream water. Nature 350:335–337

Dawson TE, Ward J, Ehleringer JR (2004) Temporal scaling of physiological responses from gas exchange to tree rings: a gender-specific study of *Acer negundo* (boxelder) under different conditions. Funct Ecol 18:212–222

DeRose RJ, Bekker MF, Wang S-Y, Buckley BM, Kjelgren RK, Bardsley T, Rittenour TM, Allen EB (2015) A millennium-length reconstruction of Bear River stream flow, Utah. J Hydrol 529:524–534

Diffenbaugh NS, Swain DL, Touma D (2015) Anthropogenic warming has increased drought risk in California. Proc Natl Acad Sci USA 112:3931–3936

Ehleringer JR (1993) Carbon and water relations in desert plants: an isotopic perspective. In: Ehleringer JR, Hall AE, Farquhar GD (eds) Stable isotopes and plant carbon/water relations. Academic Press, San Diego, pp 155–172

Ehleringer JR, Cerling TE (1995) Atmospheric $CO_2$ and the ratio of intercellular to ambient $CO_2$ concentration in plants. Tree Physiol 15:105–111

Farquhar GD, O'Leary MH, Berry JA (1982) On the discrimination between carbon isotope discrimination and the intercellular carbon dioxide concentration in leaves. Aust J Plant Physiol 9:121–137

Fischer EM, Knutti R (2015) Anthropogenic contribution to global occurrence of heavy-precipitation and high-temperature extremes. Nat Clim Change 5:560–564

Flanagan LB, Comstock JP, Eheringer JR (1991) Comparison of modeled and observed environmental influences on the stable oxygen and hydrogen isotope composition of leaf water in *Phaseolus vulgaris* L. Plant Physiol 96:588–596

Francis JA, Vavrus SJ (2012) Evidence linking Arctic amplification to extreme weather in mid-latitudes. Geophys Res Lett 39:L06801

Griffin D, Anchukaitis KJ (2014) How unusual is the 2012–2014 California drought? Geophys Res Lett 41:9017–9023

Grissino-Mayer HD (2001) Evaluating crossdating accuracy: a manual and tutorial for the computer program COFECHA. Tree Ring Res 57:205–221

Higley MC, Conroy JL, Schmitt S (2018) Last millennium meridional shifts in hydroclimate in the central tropical Pacific. Paleoceanogr Paleoclim. https://doi.org/10.1002/2017PA003233

Holmes R (1983) Computer assisted quality control in tree-ring dating and measurement. Tree Ring Bull 44:69–75

Horton RM, Mankin JS, Lesk C, Coffel E, Raymond C (2016) A review of recent advances in research on extreme heat events. Curr Clim Change Rep 2:242

Johnstone J, Dawson TE (2010) Climatic context and ecological implications of summer fog decline in the coast redwood region. Proc Natl Acad Sci 107:4533–4538

Johnstone JA, Roden JS, Dawson TE (2013) Oxygen and carbon stable isotopes in coast redwood tree rings respond to spring and summer climate signals. J Geophys Res Biogeosci 118:1–13

Kornhuber K, Petoukhov V, Petri S, Rahmstorf S, Coumou D (2016) Evidence for wave resonance as a key mechanism for generating high-amplitude quasi-stationary waves in boreal summer. Clim Dyn. https://doi.org/10.1007/s00382-016-3399-6

Leavitt SW, Danzer SR (1993) Methods for batch processing small wood samples to holocellulose for stable-carbon isotope analysis. Anal Chem 65:87–89

Lehmann J, Coumou D, Frieler K (2015) Increased record-breaking precipitation events under global warming. Clim Change 132:501–515

Liu Y, Cobb KM, Song H, Li Q, Li C-Y, Nakatsuka T, An Z, Zhou W, Cai Q, Li J, Leavitt SW, Sun C, Mei R, Chuan-Chou S, Chan M-H, Sun J, Yan L, Lei Y, Ma Y, Li X, Chen D, Linderholm HW (2017) Recent enhancement of central Pacific El Niño variability relative to last eight centuries. Nat Commun 8:15386

Loader NJ, Young GHF, Grudd H, McCarroll D (2013) Stable carbon isotopes from Torneträsk, northern Sweden provide a millennial length reconstruction of summer sunshine and its relationship to Arctic Oscillation. Quat Sci Rev 62:97–113

Malevich SB, Woodhouse CA, Meko DM (2013) Tree-ring reconstructed hydroclimate of the Upper Klamath basin. J Hydrol 495:13–22

Mann MM, Rahmstorf S, Kornhuber K, Steinman BA, Miller SK, Coumou D (2017) Influence of anthropogenic climate change on planetary wave resonance and extreme weather events. Sci Rep 7:45242

McAfee SA (2016) Uncertainty in Pacific decadal oscillation indices does not contribute to teleconnection instability. Int J Climatol 37:3509–3516

McCabe GJ, Dettinger MD (1999) Decadal variations in the strength of ENSO teleconnections with precipitation in the western United States. Int J Climatol 19:1399–1410

McCarroll D, Loader NJ (2004) Stable isotopes in tree rings. Quat Sci Rev 23:771–801

McLaughlin BC, Ackerly DD, Zion Klos P, Natali J, Dawson TE, Thompson SE (2017) Hydrologic refugia, plants, and climate change. Glob Change Biol 23:2941–2961

Meko DM, Therrell MD, Baisan CH, Hughes MK (2001) Sacramento river flow reconstruct to A.D. 869 from tree rings. J Am Water Resour Assoc 37:1029–1038

Meko DM, Woodhouse CA, Morino K (2012) Dendrochronology and links to streamflow. J Hydrol 412–413:200–209

Mooney HA, Dawson TE (2015) Northern forest ecosystems (Chapter 26). In: Zavaleta E, Mooney H (eds) Ecosystems of California. University of California Press, California

Newman M, Alexander MA, Ault TR, Cobb KM, Deser C, Di Lorenzo E, Mantua NJ, Miller AJ, Minobe S, Nakamura H, Schneider N, Vimont DJ, Phillips AS, Scott JD, Smith CA (2016) The Pacific decadal oscillation revisited. J Clim 29:4399–4427

PAGES 2k Network (2013) Continental-scale temperature variability during the past two millennia. Nat Geosci 6:339–346

Petoukhov V, Petri S, Rahmstorf S, Coumou D, Kornhuber K, Schellnhuber HJ (2016) Role of quasiresonant planetary wave dynamics in recent boreal spring-to-autumn extreme events. Proc Natl Acad Sci 113:6862–6867

R Core Team (2017) R: a language and environment for statistical computing. R Foundation for Statistical Computing, Vienna. http://www.R-project.org/

Robeson SM (2015) Revisiting the recent California drought as an extreme value. Geophys Res Lett 42:6771–6779

Roden JS (2008) Cross-dating of tree ring $\delta^{18}$O and $\delta^{13}$C time series. Chem Geol 252:72–79

Roden JS, Ehleringer JR (1999) Observations of hydrogen and oxygen isotopes in leaf water confirm the Craig-Gordon model under wide-ranging environmental conditions. Plant Physiol 120:1165–1173

Roden JS, Ehleringer JR (2007) Summer precipitation influences the stable oxygen and carbon isotopic composition of tree-ring cellulose in *Pinus ponderosa*. Tree Physiol 27:491–501

Roden JS, Lin G, Ehleringer JR (2000) A mechanistic model for interpretation of hydrogen and oxygen isotope ratios in tree-ring cellulose. Geochim Cosmochim Acta 64:21–35

Roden JS, Johnstone JA, Dawson TE (2009) Intra-annual variation in the stable oxygen and carbon isotope ratios of cellulose in tree rings of coast redwood (Sequoia sempervirens). Holocene 19:189–197

Roden JS, Johnstone JA, Dawson TE (2011) Regional and watershed-scale coherence in the stable oxygen and carbon isotope ratio time series in tree rings of coast redwood (*Sequoia sempervirens*). Tree Ring Res 67:71–86

Screen JA, Simmonds I (2014) Amplified mid-latitude planetary waves favour particular regional weather extremes. Nat Clim Change 4:704–709

Seager R, Hoerling M, Schubert S, Wang H, Lyon B, Kumar A, Nakamura J, Henderson N (2015) Causes of the 2011–14 California drought. J Clim 28:6997–7024

Sigl M, Winstrup M, McConnell JR, Welten KC, Plunkett G, Ludlow F, Büntgen U, Caffee M, Chellman N, Dahl-Jensen D, Fischer H, Kipfstuhl S, Kostick C, Maselli OJ, Mekhaldi F, Mulvaney R, Muscheler R, Pasteris DR, Pilcher JR, Salzer M, Schüpbach S, Steffensen JP, Vinther BM, Woodruff TE (2015) Timing and climate forcing of volcanic eruptions for the past 2,500 years. Nature 523:543–549

Sparks JP, Ehleringer JR (1997) Leaf carbon isotope discrimination and nitrogen content for riparian trees along elevational transects. Oecologia 109:362–367

Stahle DW, Cook ER, Cleaveland MK, Therrell MD, Meko DM, Grissino-Mayer HD, Watson E, Luckmann BH (2000) Tree-ring data document 16th century megadrought over North America. Eos 81:121–125

Sternberg LSL (1989) Oxygen and hydrogen isotope measurements in plant cellulose analysis. In: Linskens HF, Jackson JF (eds) Modern methods of plant analysis, vol 10. Plant fibers. Springer, Heidelberg, pp 89–99

Tipple BJ, Berke MA, Doman CE, Khachaturyan S, Ehleringer JS (2013) Leaf-wax *n*-alkanes record the plant-water environment at leaf flush. Proc Natl Acad Sci USA 110:2659–2664

Trenberth KE, Fasullo JT, Shepherd TG (2015) Attribution of climate extreme events. Nat Clim Change 5:725–730

Vieira LEA, Solanki SK (2010) Evolution of the solar magnetic flux on time scales of years to millenia. Astron Astrophys 509:A100

Vinnichenko NK (1970) The kinetic energy spectrum in the free atmosphere—1 second to 5 years. Tellus 22:158–166

Wang S-Y, Hipps L, Gillies RR, Yoon J-H (2014) Probable causes of the abnormal ridge accompanying the 2013–14 California drought: ENSO precursor and anthropogenic warming. Geophys Res Lett 41:3220–3226

Wang S-Y, Yoon J-H, Becker E, Gillies R (2017) California from drought to deluge. Nat Clim Change 7:465–468

Ward JK, Dawson TE, Ehleringer JR (2002) Responses of *Acer negundo* genders to inter-annual differences in water availability determined from carbon isotope ratios of tree ring cellulose. Tree Physiol 22:339–346

Ward JK, Harris JM, Cerling TE, Wiedenhoeft A, Lott MJ, Dearing M-D, Coltrain JB, Ehleringer JR (2005) Carbon starvation in glacial trees recovered from the La Brea tar pits, southern California. Proc Natl Acad Sci USA 102:690–694

Williams AP, Seager R, Abatzoglou JT, Cook B, Smerdon JE, Cook ER (2014) Contribution of anthropogenic warming to California drought during 2012–2014. Geophys Res Lett 42:6819–6828

Yamaguchi DK (1991) A simple method for cross-dating increment cores from living trees. Can J For Res 21:414–416

Yoon J-H, Wang S-Y, Gillies RR, Kravitz B, Hipps L, Rasch PJ (2015) Increasing water cycle extremes in California and in relation to ENSO cycle under global warming. Nat Commun 6:8657

Young GHF, McCarroll D, Loader NJ, Gage MH, Kirchhefer AJ, Demmler JC (2012) Changers in atmospheric circulation and Arctic Oscillation preserved within millennial length reconstruction of summer cloud cover from northern Fennoscandia. Clim Dyn 39:495–507

Young DJN, Stevens JT, Earles JM, Moore J, Ellis A, Jirka AL, Latimer AM (2017) Long-term climate and competition explain forest mortality patterns under extreme drought. Ecol Lett 20:78–86

Kahmen A, Sachse D, Arndt SK, Tu KP Farrington H, Vitousek PM, Dawson TE (2011) Cellulose $\delta^{18}$O is an index of leaf-to-air vapor pressure difference (VPD) in tropical plants. Proc Natl Acad Sci 108:1981–1986